

# Linearized Perturbations of a Black Hole: Continuum Spectrum

P.T. Leung, Alec Maassen van den Brink,\* K.W. Mak, and K. Young  
*Physics Department, The Chinese University of Hong Kong, Hong Kong, China*  
(Dated: February 8, 2020)

Linearized perturbations of a Schwarzschild black hole are described, for each angular momentum  $\ell$ , by the well-studied discrete quasinormal modes (QNMs), and in addition a continuum. The latter is characterized by a cut strength  $q(\gamma>0)$  for frequencies  $\omega = -i\gamma$ . We show that (a)  $q(\gamma\downarrow 0) \propto \gamma$ , (b)  $q(\Gamma) = 0$  at  $\Gamma = (\ell+2)!/[6(\ell-2)!]$ , and (c)  $q(\gamma)$  oscillates with period  $\sim 1$  ( $2M \equiv 1$ ). For  $\ell = 2$ , a pair of QNMs are found beyond the cut on the unphysical sheet very close to  $\Gamma$ , leading to a large dipole in the Green's function *near*  $\Gamma$ . For a source near the horizon and a distant observer, the continuum contribution relative to that of the QNMs is small.

PACS numbers: 04.30.-w, 04.70.Bw, 04.20.Jb, 11.30.Pb

## I. INTRODUCTION

Gravitational waves propagating on a Schwarzschild background probe the nontrivial spacetime around the event horizon. If and when detected [1], their signature may confirm that black holes exist. Because waves escape to infinity and into the horizon, the system is dissipative, and described by its spectrum in the lower half frequency plane—of interest both for signal interpretation and in its own right. The discrete quasinormal modes (QNMs) have been thoroughly studied [2–5]; this paper characterizes the continuum, about which little is hitherto known.

For a black hole of mass  $M$  (below  $c = G = 2M = 1$ ) and each angular momentum  $\ell$ , the radial functions  $\psi$  of scalar ( $s=0$ ) or electromagnetic ( $s=1$ ) waves and axial gravitational perturbations ( $s=2$ ) are governed by a generalized Klein–Gordon or so-called Regge–Wheeler equation (KGE or RWE)  $[d_x^2 + \omega^2 - V(x)]\psi(x, \omega) = 0$ ;  $x = r + \ln(r-1)$  is the tortoise coordinate and  $r$  the circumferential radius. The potential

$$V(r) = \left(1 - \frac{1}{r}\right) \left[ \frac{\ell(\ell+1)}{r^2} + \frac{1-s^2}{r^3} \right], \quad (1.1)$$

describing scattering by the background [6], behaves as  $V_\ell(x \rightarrow \infty) \equiv V(x) - \ell(\ell+1)/x^2 \sim 2\ell(\ell+1)\ln x/x^3$  and  $V(x \rightarrow -\infty) \sim [\ell(\ell+1) + 1 - s^2] e^{x-1}$ . We impose outgoing-wave conditions (OWCs)  $\psi(x \rightarrow \pm\infty, \omega) \sim e^{i\omega|x|}$ . (For  $x \rightarrow -\infty$ , waves thus go into the horizon.)

Polar gravitational perturbations are governed by the Zerilli equation (ZE) [7], which is the KGE with the potential  $\tilde{V}(x) = V(x) + 2d_x W(x)$ , where

$$W(r) = \Gamma + \frac{3(r-1)}{r^2(2\nu r + 3)}, \quad (1.2)$$

$\Gamma = (\ell+2)!/[6(\ell-2)!] = \frac{2}{3}\nu(\nu+1)$ , and  $\nu = \frac{1}{2}(\ell-1)(\ell+2)$ . In fact,  $W(x) = -g'(x, i\Gamma)/g(x, i\Gamma)$  [cf. below (C5)];  $g(x, \omega)$  is defined in general below. The solutions  $\psi$  of the RWE and  $\tilde{\psi}$  of the ZE are related by “intertwining” or supersymmetry (SUSY):  $\tilde{\psi}(x, \omega) = [d_x + W(x)]\psi(x, \omega)$  [2, 8, 9]. Thus, also the two continua are closely related.

The signal  $\psi(x, t \geq 0)$  depends on  $\{\psi(y, 0), \dot{\psi}(y, 0)\}$  through the Green's function  $G(x, y; t) = \int(d\omega/2\pi) \times$

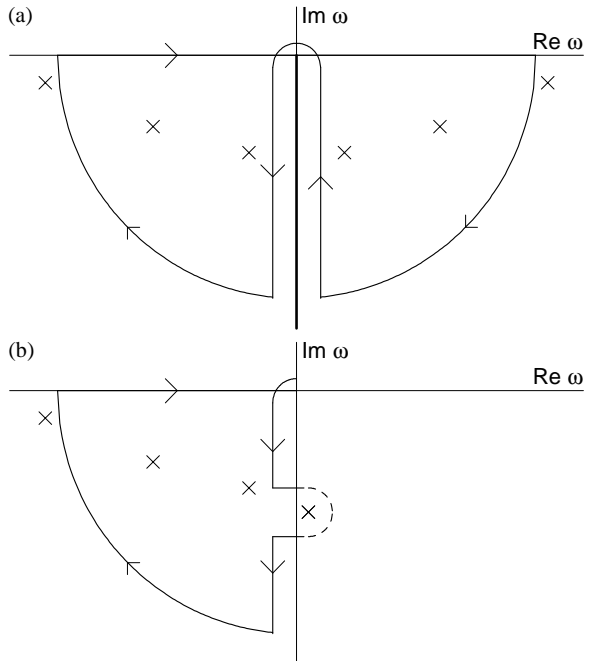


FIG. 1: Fourier inversion of  $\bar{G}$ ; crosses denote poles in the  $\omega$ -plane. (a) Conventional contour involving a cut on the NIA. (b) Modified contour detouring around the unconventional pole near  $\Gamma$  (contour on unphysical sheet shown as broken line). For simplicity the mirror contour is not shown.

$\bar{G}(x, y; \omega)e^{-i\omega t}$ . Closing the contour in the lower half  $\omega$ -plane (Fig. 1a) separates  $\bar{G}$  into (a) the large semicircle ( $|\omega| \rightarrow \infty$ ), giving a prompt signal propagating directly from  $y$  to  $x$  and vanishing after a finite  $t$  [10, 11]; (b) the QNM poles, giving rise to a ringing signal dominating at intermediate  $t$  [12, 13]; and (c) our main focus, the cut on the negative imaginary axis (NIA)  $\omega = -i\gamma$ :

$$\Delta\bar{G}(x, y; -i\gamma) = \bar{G}_+(x, y; -i\gamma) - \bar{G}_-(x, y; -i\gamma), \quad (1.3)$$

where  $\bar{G}_\pm(-i\gamma) = \lim_{\epsilon \downarrow 0} \bar{G}(-i\gamma \pm \epsilon)$  are continuations from  $\pm\omega > 0$ . The physical sheet for  $\bar{G}_+$  ( $\bar{G}_-$ ) lies to the right (left) of the NIA. [However, the opposite sides are unphysical only for the conventional choice of the cut, as in (1.3) and Fig. 1a.] The continuum is given by  $\Delta\bar{G}$ ,

and for  $\gamma \rightarrow 0$  causes the late- $t$  behavior [10, 12].

In general, the Green's function  $\bar{G}(x, y) = \bar{G}(y, x)$  is

$$\bar{G}(x, y; \omega) = \frac{f(y, \omega)g(x, \omega)}{J(g, f; \omega)}, \quad y < x, \quad (1.4)$$

where  $f$  ( $g$ ) solves the KGE with the left (right) OWC, and  $J(g, f; \omega) = gf' - fg'$  is their Wronskian. Although  $\bar{G}$  is normalization-independent, for definiteness we define  $f(x \rightarrow -\infty, \omega) \sim 1 \cdot e^{-i\omega x}$  and  $g(x \rightarrow \infty, \omega) \sim 1 \cdot e^{i\omega x}$  (adopted for  $\text{Im } \omega \geq 0$ , and continued to  $\text{Im } \omega < 0$ ). At a zero of  $J$ ,  $f \propto g$  satisfies both OWCs and defines a QNM. These are well understood, and we turn to cuts.

If  $V$  has its support in say  $[-d, d]$ , the OWCs can be imposed at  $\pm d$ , so the KGE is integrated over a finite distance; hence,  $f, g$  are analytic in  $\omega$ . The same holds if  $V$  decays faster than exponentially. If however  $V(x \rightarrow -\infty) \sim \sum_k v_k e^{\lambda k x}$  (here  $\lambda = 1$ ), typically  $f$  has poles (“anomalous points”) at  $\omega_n = -in\lambda/2$  (readily shown by Born approximation, i.e., a power series in  $e^x$ ). These are removable by scaling  $f(\omega) \mapsto \chi(\omega) = (\omega - \omega_n)f(\omega)$ , leaving  $\bar{G}$  unaffected [14]. However,  $\{v_k\}$  could conspire to “miraculously” make some  $\omega_n$  non-singular. For the RWE,  $n = N \equiv 2\Gamma$  ( $= 8$  for  $\ell = 2$ ) is miraculous. Although miracles can be studied by finite-order Born approximation, here an exact solution exists at  $\Gamma$  [cf. (1.2) and (C3)], the only miraculous point (for any  $\ell$ ) [15].

On the other hand, for  $x \rightarrow +\infty$ , the centrifugal barrier does not scatter and has no real effects [10], so we should consider the next asymptotic term

$$V_\ell(x \rightarrow \infty) \sim \frac{\ln x}{x^3} = \int_0^\infty d\lambda (3 - 2\gamma_E - \ln \lambda) \lambda^2 e^{-\lambda x} \quad (1.5)$$

( $\gamma_E$  is Euler's constant). The superposition of exponentials spreads the poles at  $-in\lambda/2$  into a cut due to the power-law tail. In  $\bar{G}$  in (1.4), only  $g$  is discontinuous and we are led to study  $\Delta g(-i\gamma) \equiv g_+(-i\gamma) - g_-(-i\gamma)$ , cf. (1.3). Section II analyzes this in terms of a position-independent cut strength  $q(\gamma)$ . The result is checked against (a) the  $\gamma \rightarrow 0$  limit, and (b) the zero and known slope at  $\gamma = \Gamma$  [15].

Section III deals with the Green's function, in particular  $\Delta\bar{G}$  and the limiting function  $\Delta\bar{G}^L$  describing propagation from near the horizon to infinity. Of course  $\Delta\bar{G} \propto q(\gamma)$  has a zero at  $\gamma = \Gamma$ ; surprisingly, there is a large contribution, approximately a dipole, *near*  $\Gamma$ , attributable to a pair of nearby QNMs on the unphysical sheet [16]. These poles are absent in  $q$  itself, and point to a relation to  $f$ —in particular to  $J$  in (1.4), which must have a zero at these positions. This leads to an analytic treatment, by linearization about  $\Gamma$ . Furthermore the  $\gamma \rightarrow 0$  behavior is examined to recover  $G(x, y; t \rightarrow \infty)$ .

Some elements of the analysis are computationally hard (CH), in a precise sense: consider the evaluation of  $g(x, -i\gamma)$  given that  $g(z \rightarrow \infty, -i\gamma) \sim e^{\gamma z}$ . If the OWC is imposed at  $x = L$ , one needs accuracy  $e^{-2\gamma L}$  to exclude an  $O(1)$  admixture of the wrong solution. If  $V$

does not have finite support ( $L \rightarrow \infty$ ) no finite accuracy suffices, defeating direct integration of the KGE [17]. Instead, one must continue from the upper half  $\omega$ -plane (where growing and decaying solutions are interchanged) to the lower one—implicit in all analytic formulas, e.g., the Born approximation or Leaver's series (see below). In contrast, evaluating a decaying function given its asymptotics, e.g.  $g(z, i\gamma) \sim e^{-\gamma z}$ , is not CH. Calculating  $g(x, \omega)$  from  $\{g(z, \omega), g'(z, \omega)\}$  is also not CH if  $|x - z|$  is finite. In Sections II and III, handling the CH parts is the technical issue. For  $z \rightarrow -\infty$ , the potential tail is exponential, and the calculation is *not* CH when matching to a finite-order Born approximation instead of to  $f(z, -i\gamma) \sim e^{-\gamma z}$  [17].

## II. CUT STRENGTH

### A. Definition and properties

On the NIA,  $g_\pm \sim 1 \cdot e^{\gamma x}$  satisfy the same RWE. Hence  $\Delta g \sim 0 \cdot e^{\gamma x}$  is the small solution  $\propto g(+i\gamma)$ . Since  $g(-\omega^*) = g^*(\omega)$ ,  $\Delta g$  is imaginary, so we introduce the real cut strength  $q$  [12, 15], to be studied numerically:

$$\Delta g(x, -i\gamma) = iq(\gamma)g(x, +i\gamma). \quad (2.1)$$

Since  $g$  is defined by the OWC at  $x \rightarrow \infty$ , (2.1) defines  $q$  independent of  $V(x)$  at any finite  $x$ : if, say,  $V_1(x > L) = V_2(x > L)$ , the corresponding  $q_1$  and  $q_2$  are identical. Leaver [12] has given a formal expression for  $q$ , which is however nontrivial to evaluate.

As a result of the SUSY relationship between the RWE and ZE, the latter's cut strength  $\tilde{q}$  obeys [15]

$$(\Gamma + \gamma)\tilde{q}(\gamma) = (\Gamma - \gamma)q(\gamma). \quad (2.2)$$

### B. Numerical evaluation

Since  $g(x, +i\gamma)$  is not CH, it is simply integrated from large  $x$ . We compute  $g(x, -i\gamma \pm \epsilon)$  by Miller's algorithm (failing at  $\epsilon = 0$ ), taking  $\epsilon \downarrow 0$  in the difference for  $\Delta g$ ; see Appendix A [18]. The solid lines in Fig. 2 show the ensuing  $q(\gamma)$  for  $\ell = 2, 3, 4$ , and are key results.

For  $\ell = 2$ ,  $q(\gamma) = 0$  at  $\gamma = 0.75, 1.35, 1.90, 2.44, 2.96, 3.48, 4.00, 4.51, 5.03, 5.54, \dots$ , suggesting that the spacing approaches  $\frac{1}{2}$ . Indeed, by a WKB analysis [19],

$$q(\gamma) \sim 4 \cos(2\pi\gamma) + O(\gamma^{-1/2}), \quad (2.3)$$

where only the correction depends on  $\ell$ . The zero at  $\Gamma$  and moreover  $q'(\Gamma) \approx -37.6$  agree with [15]

$$\begin{aligned} q'(\Gamma) &= -\frac{45\pi}{137438953472} (2100027e^8 + 30148389005) \\ &= -37.45 \dots, \end{aligned} \quad (2.4)$$

confirming both (2.4) and our numerical accuracy.

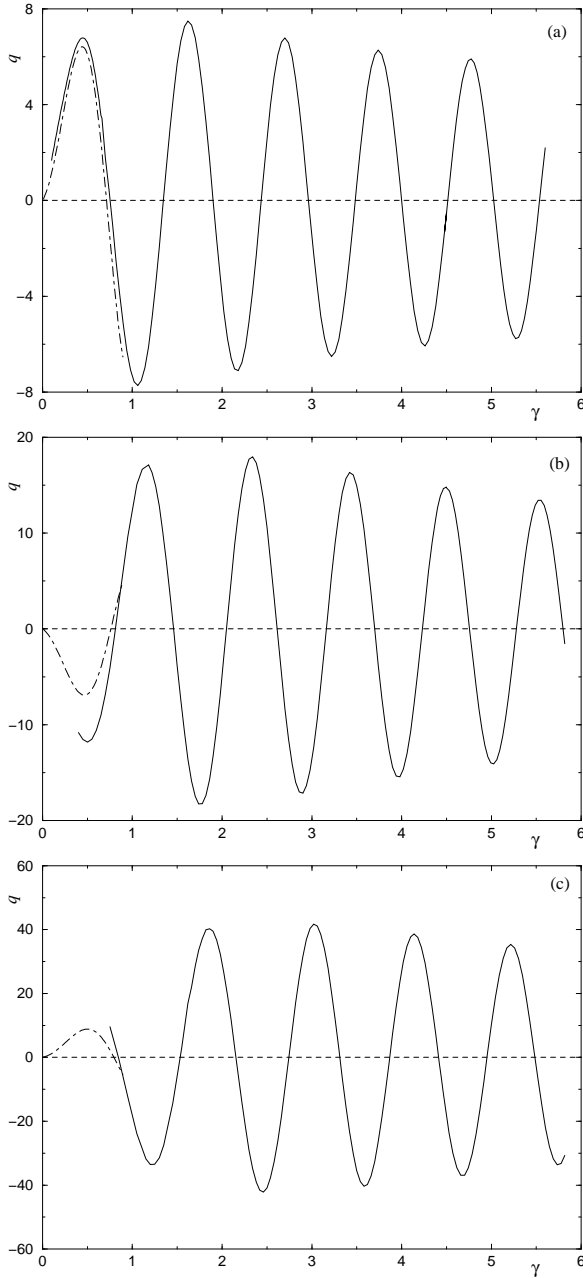


FIG. 2: Plots of  $q(\gamma)$  for (a)  $\ell = 2$ , (b)  $\ell = 3$ , and (c)  $\ell = 4$ . The solid (broken) lines are the numerical result (analytic approximation).

For  $\ell = 3, 4$ ,  $q(\gamma)$  is similarly oscillatory, but the range of validity does not include  $\Gamma$  ( $= 20$  and  $60$  respectively).

For  $\ell \rightarrow \infty$ , one has  $q'(\Gamma) \sim -\sqrt{96\pi^3}$  [20], of the same order as (2.4). Thus, in each of the analytically accessible regimes  $\gamma \downarrow 0$  [below (2.5)],  $\gamma \rightarrow \Gamma$ , and  $\gamma \rightarrow \infty$  [cf. (2.3)],  $q(\gamma)$  has a finite limiting behavior for large  $\ell$ , consistent with no new features developing in these curves.

### C. Analytic approximation

Small  $\gamma$  relates to late- $t$  behavior, controlled by (a) many finite- $r$  scatterings, whose effect vanishes exponentially, and (b) a few large- $r$  scatterings, which therefore dominate. In terms of  $u(r) \equiv \sqrt{1-1/r}\psi(r)$ , the RWE reads  $d_r^2 u + P u = 0$  [21], where  $P(r) = [r/(r-1)]^2[\omega^2 + r^{-3} - \frac{3}{4}r^{-4} - V(r)]$ ; the ZE follows in complete analogy. For large  $r$ , both  $P$  and  $\tilde{P}$  can be approximated by  $P_0(r) = \omega^2 + 2\omega^2 r^{-1} + [3\omega^2 - \ell(\ell+1)]r^{-2}$ , with errors  $P(r) - P_0(r) \sim b_3 r^{-3}$ ,  $\tilde{P}(r) - P_0(r) \sim \tilde{b}_3 r^{-3}$ . For  $s=2$ ,  $b_3 = 4\omega^2 - 2\nu + 2 < 0$  for small  $\omega$ , so  $\tilde{b}_3 = b_3 + 6/\nu$  has the smaller magnitude. Thus we regard the equation with  $P_0$  as an approximation for the ZE, and obtain results for the RWE through SUSY (2.2).

Re-expressing the above in terms of  $\psi$ , the leading  $\tilde{V}_\ell(x) \sim x^{-3} \ln x$  is reproduced exactly. The error is  $\sim x^{-3}$ , apparently down by only a factor  $\ln x \sim \ln t$ , but a pure  $x^{-3}$  term does *not* generate a late- $t$  tail to first Born approximation [10]. Thus the leading correction is an extra power of  $x^{-1} \sim t^{-1}$  (up to logarithms).

The equation with  $P_0$  is the hydrogen problem with fractional angular momentum. The OWC for  $r \rightarrow \infty$  selects its confluent-hypergeometric solution [22] and the branch of  $\sqrt{-\omega^2}$ , giving  $\tilde{u}(r, \omega) \approx (-2i\omega)^{\sigma-i\omega} r^\sigma e^{i\omega r} \times U(\sigma-i\omega, 2\sigma; -2i\omega r)$  with  $2\sigma \equiv 1 + \sqrt{(2\ell+1)^2 - 12\omega^2}$ .

Since we consider  $\gamma \rightarrow 0$  at fixed  $r$ ,  $-i\omega r \approx 0$ , so

$$\tilde{q}(\gamma) = \frac{\Delta \tilde{u}(r, -i\gamma)}{i\tilde{u}(r, i\gamma)} \approx -2 \frac{\Gamma(\sigma+\gamma)}{\Gamma(\sigma-\gamma)} \frac{\sin[\pi(\sigma+\gamma)]}{(2\gamma)^{2\gamma}}, \quad (2.5)$$

with  $\Gamma$  the Gamma function (not the special frequency). This approximation is shown by broken lines in Fig. 2. In particular, it shows that  $q'(0) = \tilde{q}'(0) = (-1)^\ell 2\pi$  [10].

## III. GREEN'S FUNCTION

### A. Evaluation and general properties

Using  $J(g_-, g_+; -i\gamma) = -2i\gamma q(\gamma)$ , one finds

$$\Delta \bar{G}(x, y; -i\gamma) = -2i\gamma q(\gamma) \frac{f(x, -i\gamma) f(y, -i\gamma)}{J_+(-i\gamma) J_-(-i\gamma)}, \quad (3.1)$$

with  $J_\pm \equiv J(g_\pm, f)$ . We evaluate  $g_\pm$  as in Section II B and use Jaffé's series for  $f$  (Appendix B). Fig. 3 shows  $-\iota \Delta \bar{G}(x, y; -i\gamma)$  for  $\ell = 2$ ; the two contrasting cases reveal a strong  $x$ - and  $y$ -dependence.

The above is the clearest, but more efficient is to rewrite (1.4) as (suppressing  $\omega = -i\gamma \pm \epsilon$ ,  $\epsilon \neq 0$ ):

$$\bar{G}(x, y) = \frac{[f(y)/f(z)][g(x)/g(z)]}{f'(z)/f(z) - g'(z)/g(z)}. \quad (3.2)$$

In principle any  $z$  will do. However, if  $\pm z \gg 1$ , both  $L(z) \equiv f'(z)/f(z)$  and  $R(z) \equiv g'(z)/g(z)$  approach  $\pm i\omega$ ,

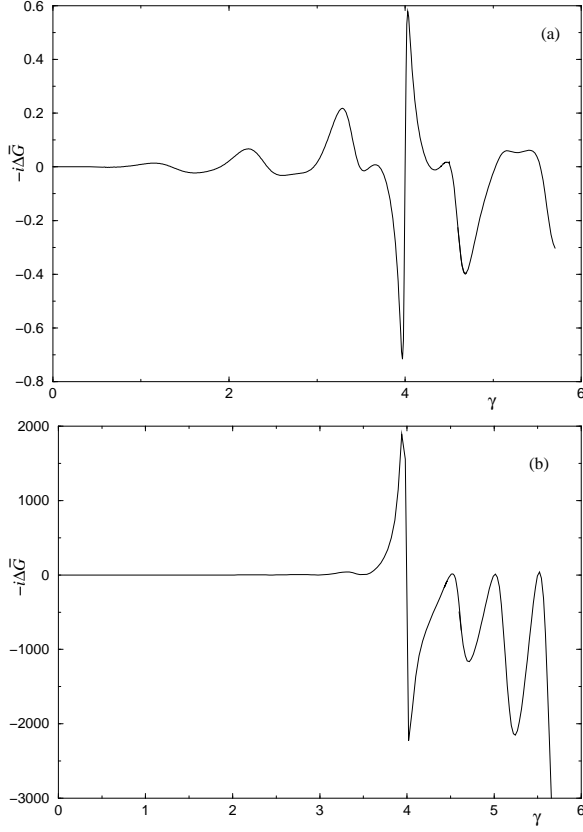


FIG. 3: Plots of  $-i\Delta\bar{G}(x, y; -i\gamma)$  for  $\ell = 2$  and (a)  $x = 0.2$ ,  $y = 0.1$ , (b)  $x = 1.0$ ,  $y = -1.0$ .

so the exponentially small denominator is hard to evaluate. Thus choose  $z \sim O(1)$  and (a) compute  $R(z)$  (Appendix A). This CH step is carried out only at *one*  $z$ . (b) Calculate  $f$  as above for  $L(z)$ . (c) Up to irrelevant normalization,  $f(y)$  and  $g(x)$  follow by integrating the KGE over finite distances, yielding  $\bar{G}$ . (d) Let  $\epsilon \downarrow 0$ . We have verified that the result agrees with (3.1).

As said below (1.3),  $\Delta\bar{G}(\gamma \approx 0)$  governs  $G(t \rightarrow \infty)$ . Since  $\gamma \downarrow 0$  relates to  $x \rightarrow \infty$  [10], one can neglect  $V_\ell$  for all factors in (3.1) except  $q(\gamma) \approx (-1)^\ell 2\pi\gamma$  (Section II C), giving  $f(x, -i\gamma) \propto x^{\ell+1}$  and  $g_\pm(x, -i\gamma) \approx [(2\ell)!/\ell!] \times (-2\gamma x)^{-\ell} e^{\gamma x}$ . This yields  $\Delta\bar{G} \approx 4\pi i [(2\ell+1)!!]^{-2} \times (-xy)^{\ell+1} \gamma^{2\ell+2}$ , elegantly reproducing [10, 12]

$$G(x, y; t) \approx 2 \frac{(2\ell+2)!}{[(2\ell+1)!!]^2} \frac{(-xy)^{\ell+1}}{t^{2\ell+3}}. \quad (3.3)$$

A potential tail  $V_\ell(x) \sim x^{-\alpha} \ln x$  generically leads to  $G \sim t^{-(2\ell+\alpha)} \ln t$ , but in some special cases (including the RWE), the  $\ln x$  factor does not lead to a  $\ln t$  factor [10].

## B. Limiting $x$ and $y$

The physically important limit is  $-y, x \rightarrow \infty$ . Because  $f(y, -i\gamma) \sim e^{-\gamma y}$  and  $f$  in general also has an outgoing

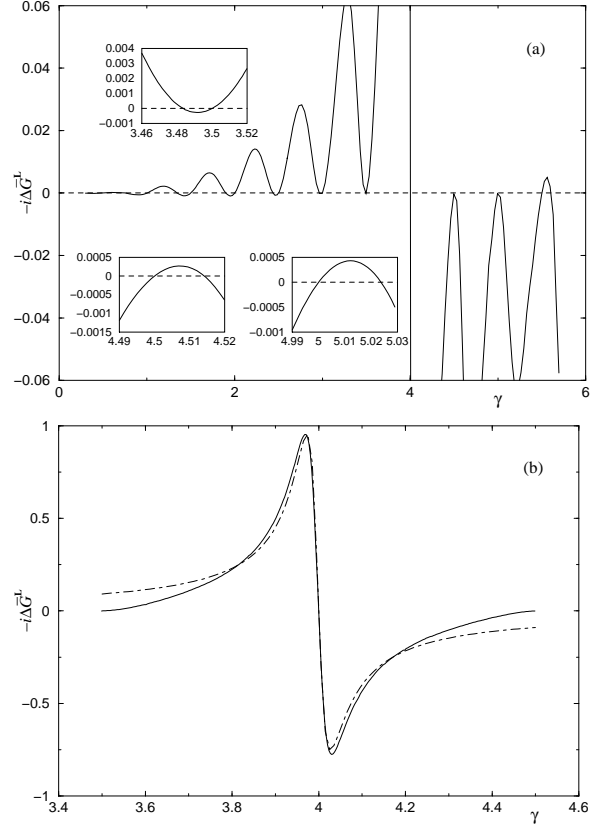


FIG. 4: Plots of  $-i\Delta\bar{G}^L(-i\gamma)$  for  $\ell = 2$ . (a) For  $0 \leq \gamma \leq 5.6$ . Insets show some regions with two close zeros. (b) The region  $\gamma \approx 4$  expanded. The solid line is the numerical result, and the broken line is a fit to (3.7) with  $a_2 = -0.0227$ .

part to the right [ $f(x, -i\gamma) \sim e^{\gamma x}$ ], there is a steep position dependence. This is simply a result of the long signal propagation time, and is removed if  $t$  is measured from the first arrival at  $t_0(x, y) \equiv x - y$ . [Closing the contour in the upper  $\omega$ -plane readily shows that  $G(t < t_0) = 0$ .] Thus, consider

$$G^L(t') \equiv \lim_{x, -y \rightarrow \infty} G(x, y; t_0 + t'), \quad (3.4)$$

with Fourier transform  $\bar{G}^L(\omega) = J(g, f; \omega)^{-1}$  by (1.4) and the normalization of  $f, g$ . The cut is

$$\Delta G^L(t') = \int_0^\infty \frac{d\gamma}{2\pi i} \Delta\bar{G}^L(-i\gamma) e^{-\gamma t'}, \quad (3.5)$$

$$\Delta\bar{G}^L(-i\gamma) = \Delta[J(g, f; -i\gamma)^{-1}] \quad (3.6)$$

[cf. (1.3) for  $\Delta$ ]. Results are shown in Fig. 4.

Although  $\Delta\bar{G}^L(-i\Gamma) = 0$ , surprisingly  $\Delta G^L$  is largest *near*  $\gamma = \Gamma$ , where it is approximately a dipole (Fig. 4b; the dominance is less pronounced if the source is displaced from the horizon, cf. Fig. 3). The solid line in Fig. 5 shows  $\Delta G^L(t')$  [obtained by integrating (3.5) up to  $\gamma = 5.60$ , hence accurate except for very small  $t'$ ].

The cut  $\Delta\bar{G}^L(-i\gamma)$  vanishes at (a) the zeros of  $q(\gamma)$  [cf. (3.1)], and (b)  $\gamma = \frac{1}{2}, 1, \frac{3}{2}, \dots$ . The former depend

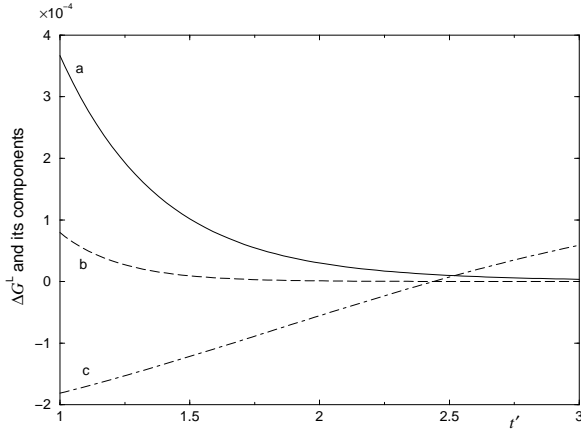


FIG. 5: Solid line (a): continuum contribution  $\Delta G^L(t')$  for  $\ell = 2$ . Dashed line (b): contribution of the pair of nearby unconventional poles. Dot-dashed line (c): corresponding contribution from the first QNM, scaled down by  $10^3$ .

only on  $V(x \rightarrow +\infty)$  [cf. below (2.1)], the latter only on  $V(x \rightarrow -\infty)$ , scaling with  $\lambda$ . If the two tails are separately adjusted the sequences are independent, but for the present  $\lambda = 1$ , sequence (a) acquires one integer member at  $\gamma = \Gamma$ . However, this member simultaneously disappears from sequence (b) [cf. above (1.5)], consistent with the first-order zero at  $\gamma = \Gamma$  in Fig. 4.

Some members of the two sequences are close, cf. the insets in Fig. 4a. The many zeros also ensure that  $\Delta \bar{G}^L$  is generically small. (Section III E contains quantitative estimates.)

### C. Poles on unphysical sheet: numerics

The behavior of  $\Delta \bar{G}^L(-i\gamma)$  for  $\gamma \approx \Gamma$  can in fact be attributed to a pair of nearby QNM poles  $\omega_{\pm}$ . Suppose  $\bar{G}_{\pm}^L(\omega) \approx (a_1 \pm ia_2)/(i\omega - 4 - b \pm ic)$ , where  $a_1, a_2, b$  are real and  $c > 0$  so  $\omega_{\pm}$  are on the unphysical sheets. In terms of  $\xi = \gamma - \Gamma$ , on the NIA one has

$$\Delta \bar{G}^L(-i\gamma) \approx \frac{2ia_2\xi}{(\xi - b)^2 + c^2}, \quad (3.7)$$

with  $a_1c + a_2b = 0$  implementing the zero at  $\gamma = \Gamma$ . The broken line in Fig. 4b shows this fit for  $\ell = 2$ , yielding

$$\omega_{\pm} + i\Gamma = \mp c - ib \approx \mp 0.027 + 0.0033i. \quad (3.8)$$

Further, a plot of  $|J_+(\zeta - i(\Gamma + b))|$  vs.  $\zeta > 0$  (not shown) clearly supports a simple zero at  $\zeta \approx -c$  [cf. (3.6)].

In summary, we have extrapolated Leaver's series to the unphysical sheet, revealing nearby poles making the largest contribution to the cut. To the best of our knowledge, this is the first time such QNMs have been found, and these obviously have more effect on the dynamics than QNMs on the physical sheet at larger  $|\text{Im } \omega|$ .

In a broader context, consider the Kerr black hole. By comparing numerics for moderately small rotation  $a$  [23]

with the QNM multiplet found analytically to branch off from  $\Gamma$  at infinitesimal  $a$ , one concludes that one *additional* multiplet has to emerge (as  $a$  increases) near  $\omega = -i\Gamma$ . Rather than the possibilities contemplated in Ref. [15], we speculate that this multiplet may be due to the unconventional poles discussed here splitting (as they must when spherical symmetry is broken) and moving through the NIA as  $a$  is tuned [24].

Thus it is advantageous to consider another Fourier contour going into the unphysical sheet and detouring around  $\omega_{\pm}$  (Fig. 1b), including them as QNM contributions (line b in Fig. 5). This slightly reduces the continuum (due to the integral along the NIA and often neglected as "background"). More importantly, suppose these poles move through the NIA as a parameter (say,  $a$ ) is tuned, becoming conventional QNMs. In the assignment of Fig. 1b, the total QNM and continuum contributions are *separately* continuous; for the conventional contour, each is discontinuous.

### D. Poles on unphysical sheet: analytics

Interestingly, the above extrapolation can also be carried out analytically, by assuming the linearization of  $J_+(\omega \approx -i\Gamma)$  to be valid up to the nearest zero,

$$\omega_{+} + i\Gamma \approx -\frac{J(-i\Gamma)}{J'_{+}(-i\Gamma)}. \quad (3.9)$$

Since  $\Delta J(-i\Gamma)$  vanishes, one does not have to indicate the sheet in the numerator. Following the methods and notation of [15], one readily obtains

$$\begin{aligned} J(-i\Gamma) &= \frac{2\nu N}{2\nu + 3} \left( \frac{\gamma_3}{\gamma_5} - 1 \right) \\ &= -\frac{700009}{917504} \quad \text{for } \ell = 2, \end{aligned} \quad (3.10)$$

with the constants

$$\begin{aligned} \gamma_3 &\equiv -\left[ \frac{9}{2} \sum_{j=0}^{N-2} \frac{N^{j+1}}{j!} + 3(2\nu+3) \frac{N^N}{(N-1)!} \right] e^{-N} \\ &= -\frac{28 \cdot 11093}{3} e^{-8} \quad \text{for } \ell = 2, \end{aligned} \quad (3.11)$$

$$\begin{aligned} \gamma_5 &\equiv \frac{3\nu N^{N+1} e^{-N}}{(1-2\nu)(\nu+1)(N-2)!} \\ &= -\frac{2^{24}}{135} e^{-8} \quad \text{for } \ell = 2 \end{aligned} \quad (3.12)$$

characterizing  $f(-i\Gamma)$  and  $g(-i\Gamma)$  respectively (cf. Appendix C). The peculiar integer in the numerator of (3.10) has already surfaced in Ref. [15].

Calculating  $J'_{+}(-i\Gamma)$  is formidable (Appendix C), but since  $\omega_{+} + i\Gamma$  in (3.8) is mostly real, one can first evaluate

only  $\text{Re } J'_+—much simpler due to the zero in  $\Delta g$ :$

$$\begin{aligned}\text{Re } J'_+(-i\Gamma) &= \frac{1}{2}\Delta J'(-i\Gamma) = -\frac{1}{2}q'(\Gamma)J\{g(i\Gamma), f(-i\Gamma)\} \\ &= -\frac{\gamma_3 q'(\Gamma)}{4\nu(2\nu+3)}.\end{aligned}\quad (3.13)$$

Ignoring the imaginary part, substitution yields

$$\begin{aligned}\omega_+ + i\Gamma &\approx \frac{8\nu^2 N}{q'(\Gamma)} \left( \frac{1}{\gamma_5} - \frac{1}{\gamma_3} \right) \\ &= -0.0328\dots \quad \text{for } \ell = 2,\end{aligned}\quad (3.14)$$

comparing favorably with the numerical  $-0.027$ , where the latter value, also found by extrapolation from the physical sheet, need not be more accurate. Taking (3.13) as an approximation for  $J'_+$  provides a bound: given that (3.14) has yielded an  $\omega_+$  close to  $-i\Gamma$ , including  $\text{Im } J'_+$  will render  $\omega_+$  even closer. Indeed, inserting into (3.9) the *exact* (C20) for  $J'_+(-i\Gamma, \ell=2)$  yields

$$\omega_+ + i\Gamma \approx -0.03248 + 0.003436i \quad (3.15)$$

as our final estimate; especially the agreement of  $\text{Im } \omega_+$  with (3.8) is remarkable.

Combining (3.5) and (3.7), our linearization of  $J$  immediately yields  $a_2 \approx \text{Re}(J'_+(-i\Gamma))^{-1} \approx -\text{Re } \omega_+/J(-i\Gamma) \approx -0.0426$ . The agreement with the numerical fit  $a_2 \approx -0.0227$  is slightly worse than the one for  $\omega_+$  itself.

For  $\ell = 3$ , the same procedure would lead to  $\omega_+ + i\Gamma \approx -0.847 + 0.0433i$ —outside the radius of convergence of the series for  $J_+(\omega)$ , which is  $\frac{1}{2}$  due to its poles at the anomalous points of  $f$ . Heuristically removing these poles by rescaling  $J$ , e.g., by linearizing  $H(\omega) \equiv J(\omega) \times \sin(2\pi i\omega)/(w+i\Gamma)$  [cf. (B4) below], does not change the prediction for  $\omega_\pm$ . Besides, the fact remains that  $J(\omega)$  has structure on a scale of  $O(1)$ . Thus, already for  $\ell = 3$ , currently there is only slight evidence for  $\omega_\pm$  near  $-i\Gamma$ . Similarly, for large  $\ell$ , the asymptotics of  $q'(\Gamma)$  given at the end of Section II B yield (3.14) as  $\omega_+ + i\Gamma \sim -0.051\Gamma$ , far outside the permitted range of extrapolation. While we have not fully studied the large- $\ell$  asymptotics of  $\text{Im } J'_+(-i\Gamma)$ , this is unlikely to change the conclusion that our calculation is valid for  $\ell = 2$  and possibly  $\ell = 3$  only.

### E. QNMs versus background

In terms of  $t'$ , also the QNM contributions can be expressed for  $x, -y \rightarrow \infty$  in a position-independent manner. The various magnitudes and phases are then completely determined—unlike the usual situation in (Q)NM analysis. Fig. 5, line c shows the contribution of the first QNM (i.e., the pair with the smallest damping, at  $\omega_1 = \pm 0.747 - 0.178i$ ), reduced by  $10^3$ . Insofar as the low QNMs are likely to be the most important for signal analysis, the comparison in Fig. 5 provides the estimate that the “background” is small.

The above numerics refer to the most important case  $\ell = 2$ . The regions near the much larger  $\Gamma(\ell \geq 3)$  are currently unattainable numerically. In any event, Section III D shows that the unconventional poles, if present at all, must be further removed from  $\Gamma$ , so their influence on the cut is likely to be less pronounced.

### F. Zerilli equation

The corresponding quantity for the ZE is trivially  $\Delta \tilde{\tilde{G}}^L(-i\gamma) = \Delta \tilde{G}^L(-i\gamma)$ , by (3.6) and  $\tilde{J} = J$  [25]. Thus, the discussion of Fig. 5 also applies to the ZE.

Since the ZE has a QNM at  $-i\Gamma$  but the RWE does not [15], it might appear that the two  $\tilde{G}^L$ ’s should have different pole structures there. Indeed,  $\tilde{G}$  does have a pole, with residue  $\propto \tilde{f}(y, -i\Gamma)\tilde{g}(x, -i\Gamma)$ . However,  $-i\Gamma$  is anomalous for the ZE (but miraculous for the RWE), so  $\tilde{f}$  does not contain the normal growing solution, eliminating the residue in  $\tilde{G}^L$ .

Physically, for a source *not* at the horizon, the axial (RWE) dynamics does *not* have a term  $e^{-\Gamma t}$ , but the polar (ZE) dynamics does—with, however, vanishing amplitude as the source approaches the horizon ( $y \rightarrow -\infty$ ).

## IV. DISCUSSION

Like the hydrogen atom in quantum mechanics, the Schwarzschild black hole is the simplest compact object in relativity, and its spectrum also contains a continuum in addition to the discrete part. We have characterized this continuum, recovering the behavior both for  $\gamma \equiv i\omega \rightarrow 0$  and near the miraculous point  $\Gamma$ . The present numerical method cannot access much larger  $\gamma$ , but the pattern already appears clear.

Although  $\Delta \tilde{G}^L(-i\Gamma) = 0$ , it surprisingly is largest *near*  $\Gamma$ . Moreover, for a limiting source and observer, the cut contribution is small relative to the QNMs—of relevance once gravitational waves are detected.

Signal analysis in terms of a  $V(x)$  is formally an inverse problem. These are well-studied for closed systems [26]: *two real* spectra determine  $V$  on a finite interval. For open systems, we conjecture that *one complex* spectrum suffices—provided the discrete QNMs are complete. The cut (rendering them incomplete) is likely to hamper inversion, but, intriguingly, the *extended* family of QNMs (including the unconventional ones) *may* be complete for the dynamics (apart from the prompt signal) and permit inversion, even though  $V$  is not finitely supported [13]. The present at least shows that *one* pair of nearby poles on the unphysical sheet already dominates the cut.

These questions may be explored through solvable models with potential tails [3, 27]. Some aspects of the RWE and ZE can also be analyzed asymptotically [19]. Numerical algorithms (e.g., generalizing the continued-fraction method [12]) valid on the NIA and even into the

unphysical region would also be useful, allowing QNMs there to be studied directly rather than through extrapolation.

Finally, it would be instructive to evaluate the continuum for a Kerr hole, to study any unconventional poles, in particular their movement and possible emergence onto the physical sheet as the rotation is increased from zero [28].

### Acknowledgments

We thank E.S.C. Ching, Y.T. Liu, W.M. Suen and C.W. Wong for many discussions, and the Hong Kong Research Grants Council for support (CUHK 4006/98P). AMB was also supported by a C.N. Yang Fellowship.

### APPENDIX A: LEAVER'S SERIES

Suppressing the parameter  $\omega$ , we first calculate an unnormalized  $\underline{g}$ . Define  $R \equiv g'/g = \underline{g}'/\underline{g}$ . Choose  $z$  and compute  $\bar{R}(z)$  by Miller's algorithm of downward recursion on Leaver's series [29, 30]. With, say,  $\underline{g}(z) \equiv 1$ ,  $\underline{g}(x)$  is then integrated trivially for all  $x$ . Thus, the norm  $\mathcal{N} = \lim_{x \rightarrow \infty} e^{i\omega x} / \underline{g}(x)$  is not CH; convergence provides a check. Finally,  $g = \mathcal{N}\underline{g}$ . This procedure requires only one CH calculation [for  $\bar{R}(z)$ ], instead of one for each  $x$ .

In principle, the result should be  $z$ -independent; in practice we take  $|z| \sim 1$ . However, we have checked that the  $R(z)$  thus obtained obey  $R' = V - \omega^2 - R^2$ . Such tests show that Miller's algorithm works well at least for  $-4.25 < \text{Im } \omega < -1.25$ ,  $10^{-4} < \text{Re } \omega < 0.1$ , and  $-0.5 < z < 1.5$ ; by optimizing  $z$ , the range on the NIA can be slightly extended to  $0.5 \lesssim \gamma \lesssim 6.0$ , varying somewhat with  $\ell$ . One also verifies that  $R(z \rightarrow \pm\infty) \rightarrow \pm i\omega$ .

In practice we calculate  $q(\gamma)$  using a small  $\epsilon \neq 0$  and some definite  $x$  in  $(-5, 0)$ ; the smaller  $\epsilon$ , the wider the range of permissible  $x$ . Convergence for  $\epsilon \rightarrow 0$  is rapid, and the  $x$ -independence in particular gives an accuracy estimate. On this basis, the decimals given in the main text should be significant, and the error bars in the figures should be tiny on the given scale.

### APPENDIX B: JAFFÉ'S SERIES

This appendix presents Jaffé's series [29, 31], with particular attention to the anomalous and miraculous points. The series, first used for the  $\text{H}_2^+$  ion and applied to the present problem by Leaver [29], expresses the outgoing solution,  $f(r \downarrow 1, \omega) \sim e^{-i\omega x} = (r-1)^{-i\omega} e^{-i\omega r}$ , as

$$f(r, \omega) = (r-1)^{-i\omega} r^{2i\omega} e^{i\omega r} \sum_{n=0}^{\infty} a_n(\omega) \left( \frac{r-1}{r} \right)^n. \quad (\text{B1})$$

The coefficients  $a_n(\omega)$  satisfy

$$\alpha_n a_{n+1} + \beta_n a_n + \gamma_n a_{n-1} = 0, \quad (\text{B2})$$

$n = 1, 2, \dots$ , with  $a_{n<0} = 0$  and ( $s = 2$  throughout)

$$\begin{aligned} \alpha_n &= (n+1)(n+1-2i\omega), \\ \beta_n &= -2n^2 + (8i\omega-2)n + 8\omega^2 + 4i\omega - \ell(\ell+1) + 3, \\ \gamma_n &= n^2 - 4i\omega n - 4\omega^2 - 4. \end{aligned} \quad (\text{B3})$$

The normalization  $a_0$  can be chosen freely (see below).

Jaffé's series leads to some important insights. First,  $\alpha_n$  has a zero at  $\omega = -i(n+1)/2$ . So at  $\omega_n = -in/2$  ( $n = 1, 2, \dots$ ),  $a_{m \geq n}$  and therefore  $f(\omega)$  generically have simple poles, removable through scaling by  $\omega - \omega_n$ , in effect killing the  $a_{m < n}$  and making  $a_{m \geq n}$  finite [15]. Then the leading behavior is  $\chi(r, \omega_n) \sim (r-1)^{n/2} \sim e^{i\omega_n x}$ , an *incoming* wave. Thus, at these anomalous points,  $f \propto \chi$  is outgoing (being the analytic continuation of outgoing waves defined for  $\text{Im } \omega > 0$ ) and incoming.

However, according to (B2),  $a_n$  (hence, all  $a_{m \geq n}$ ) can be non-singular even when  $\alpha_{n-1} = 0$ , if  $\beta_{n-1} a_{n-1} + \gamma_{n-1} a_{n-2} = 0$ . This is called a miracle; in the present case for  $\ell = 2$ , it occurs at  $n = 8$ , i.e., at  $\omega = -i\Gamma$  [15].

Because of the poles at the anomalous but not at the miraculous  $\omega_n$ , we choose to calculate  $\chi$  with

$$a_0 = \frac{\sin 2\pi\gamma}{\gamma - \Gamma}, \quad (\text{B4})$$

in which case all functions are nonsingular at any  $\omega_n$  (both anomalous and miraculous). However, if needed [e.g. in (3.6)] we can always find the normalization by taking  $r \downarrow 1$ ; cf. Appendix A.

Finally, note that  $f(\omega)$  has no cut in the  $\omega$ -plane, as is also evident from more general considerations.

### APPENDIX C: FREQUENCY DERIVATIVE OF THE WRONSKIAN

#### 1. Preliminaries

Writing  $f_1 \equiv \partial_\omega f(\omega)|_{-i\Gamma}$  and similar for  $g$ , we are interested in (arguments  $-i\Gamma$  suppressed where possible)

$$J'_+ = g_{1+} d_x f + g d_x f_1 - f_1 d_x g - f d_x g_{1+}. \quad (\text{C1})$$

The differentiated RWE

$$[d_x^2 - \Gamma^2 - V(x)] f_1(x) = 2i\Gamma f(x) \quad (\text{C2})$$

etc., plus nontrivial differentiated OWCs, determines  $f_1$  and  $g_{1+}$ . The calculation proceeds in  $r$ , using  $x(r)$  as a shorthand only. One introduces the SUSY generator

$$\xi_1(r) = \frac{2\nu r + 3}{r} e^{-Nx/2} \quad (\text{C3})$$

and the secondary solution  $\xi_2(r) = \xi_1(r) \int_1^r dt [t/(t-1)] \times \xi_1^{-2}(t)$ , where the integral is elementary [15]:

$$\begin{aligned} \frac{\xi_2(r)}{\xi_1(r)} &= \frac{1}{\gamma_5} \left[ e^{N(r-1)} \sum_{j=0}^{N-2} \frac{[N(1-r)]^j}{j!} - 1 \right] \\ &\quad + \frac{e^{Nr}(r-1)^{N-1} [2\nu r^2 - (2\nu+3)r + 6]}{4\nu^2 N(2\nu r + 3)}. \end{aligned} \quad (\text{C4})$$

Note that the decay of  $\xi_2$  near the horizon is due to a high-order cancellation, cf. the first line of (C4). This behavior complicates the entire calculation, right down to the floating-point evaluation of (C20) or its higher- $\ell$  counterparts. Namely, for  $\ell = 2$  ( $\ell = 3$ ) the first 3 (16) digits cancel in the rational and transcendental [largely  $\propto \text{Ei}(N)$ ] contributions to  $\text{Im } J'_+$ , so that very high accuracy is needed already for moderate  $\ell$ .

The Wronskian is readily evaluated as

$$J(\xi_1, \xi_2) = 1. \quad (\text{C5})$$

With  $\xi_j \equiv \xi_1 + \gamma_j \xi_2$ , the outgoing functions are  $f = \xi_3/(2\nu + 3)$  and  $g = 2\nu N \xi_5/\gamma_5$ , while the incoming ones read  $f(i\Gamma) = (2\nu + 3)N \xi_2$  and  $g(i\Gamma) = \xi_1/(2\nu)$ ; the latter has been used already in deriving the final line of (3.13).

## 2. Differentiated wave functions

Using a Green's function approach, (C2) is solved as

$$f_1(r) = \frac{iN}{2\nu + 3} \left[ \xi_2(r) \int^r dt \frac{t\xi_1(t)\xi_3(t)}{t-1} - \xi_1(r) \int^r dt \frac{t\xi_2(t)\xi_3(t)}{t-1} \right], \quad (\text{C6})$$

where the undetermined integration constants reflect the possibility of adding a homogeneous solution to (C2). Of course,  $f_1$  itself is not arbitrary, and the second of these constants follows from  $f_1(x \rightarrow -\infty) \sim [-ix + O(e^x)]e^{-\Gamma x}$ . The required asymptotics of the integrals in (C6) are straightforward; for definiteness we write the answer as

$$iN^{-1}(2\nu+3)f_1 = \xi_1\{B + N^{-1}x + \gamma_3 D - N^{-2}\} - \xi_2\{C + \gamma_3[B+N^{-1}x] + \beta\}; \quad (\text{C7})$$

$$B(r) = \int_1^r dt \frac{t}{t-1} [\xi_1(t)\xi_2(t) - N^{-1}], \quad C(r) = \int_\infty^r dt \frac{t\xi_1^2(t)}{t-1}, \quad D(r) = \int_1^r dt \frac{t\xi_2^2(t)}{t-1}. \quad (\text{C8})$$

The integrals (C8) can be evaluated by partial-fraction expansion, yielding only elementary functions plus  $\text{Ei}(r) \equiv \int_{-\infty}^r dt e^t/t$  [32]. However, the full primitives are cumbersome—not surprising since already  $\xi_2$  is involved. Hence, we only give results when required.

One cannot find  $\beta$  from low-order asymptotics, as was the case for  $\gamma_3$  in the calculation of  $f$  itself [15]. For

$\ell = 2$ , we have obtained the Born series for  $f(r \approx 1, \omega)$  by computer algebra. Only after  $\partial_\omega$  is taken in each term does one set  $\omega = -i\Gamma$ , comparing the result to the analogous expansion of (C7). The first eight terms agree, as they must. The ninth  $[O((r-1)^4)]$  terms agree if

$$\beta = 9 \text{Ei}(-8) + \frac{\gamma_3}{4}(\gamma_E + \ln 8) + \frac{4226209}{60} e^{-8}, \quad (\text{C9})$$

and for this value the two series coincide. The transcendental  $\text{Ei}$ ,  $\gamma_E$ , and  $\ln 8$  only occur to cancel their counterparts in the expansion of  $C(r)$ , defined with a lower limit  $r = \infty$  to ensure convergence—the Born series for  $f_1$  essentially involves rationals only. Indeed,  $\text{Ei}(-8)$  does not occur in (C20) below.

For general  $\ell$ , we calculate  $\beta$  by requiring that  $\partial_\omega^2[(r-1)^{i\omega} f(r, \omega)]_{-i\Gamma}$  be single-valued near  $r = 1$ . This generalizes the determination of  $\gamma_3$  and hence  $f$  in [15], by demanding that  $f_1(r) + if(r) \ln(r-1)$  be a power series near  $r = 1$ . Using the latter, presently we find that

$$f_2(r) - 2iN^{-1}f_1(r) + 2if_1(r) \ln(r-1) + [2N^{-1} - \ln(r-1)]f(r) \ln(r-1) \quad (\text{C10})$$

should not involve  $\ln(r-1)$ . The equation for  $f_2$  analogous to (C2) yields [cf. (C6)]

$$f_2(r) - \frac{2i}{N}f_1(r) = 2iN \left[ \xi_2(r) \int^r dt \frac{t\xi_1(t)f_1(t)}{t-1} - \xi_1(r) \int^r dt \frac{t\xi_2(t)f_1(t)}{t-1} \right]. \quad (\text{C11})$$

Insertion into (C10) using (C7) for  $f_1$  throughout eventually yields that all logarithms indeed cancel if

$$\beta = 9 \text{Ei}(-N) - \frac{(18\nu+9)\gamma_5}{4\nu^2 N^2} + \frac{2\gamma_3}{N} \left[ \gamma_E + \ln N + \frac{1}{N} \right] + \sum_{j=1}^{N-1} \frac{9}{j} \left[ e^{-N} \sum_{k=j}^{N-2} \frac{N^k}{k!} - \frac{\gamma_5}{2\nu^2 N} \right] + N\rho. \quad (\text{C12})$$

The residue  $\rho \equiv \text{res}[r\xi_1^2(r)B(r)/(r-1)]_{r=1}$  reads

$$\rho = (2\nu+3)^2 c_N + (9-4\nu^2) c_{N-1} + 9 \sum_{p=1}^{N-2} c_p, \quad (\text{C13})$$

$$\begin{aligned}
\frac{\gamma_5 e^{2N} c_p}{N^p} = & 2\gamma_3 e^N \sum_{j=1}^p \left( \frac{N^j}{j!} - 1 \right) \frac{N^{-j-1}}{j(p-j)!} - \sum_{j=1}^p \sum_{k=0}^{j-1} \frac{9N^{k-j}}{j(p-j)!k!} + \frac{(2\nu+3)^2 N^{N-1}}{(N+p)!} (2^{N+p} - 1) \\
& - \frac{(2\nu+3)^2 N^{N-2}}{p!(N-1)!} + \sum_{j=1}^{N-1} \left( \frac{(j-1)!2^{p+j}}{(p+j)!} - \frac{1}{jp!} \right) \left\{ 9 \sum_{k=j}^{N-2} \frac{N^k}{k!} + 6(2\nu+3) \frac{N^{N-1}}{(N-1)!} \right\} \\
& + \sum_{j=1}^{N-1} \frac{1}{j(p+j)!} \left\{ \frac{4\nu^2 N^{N-1}}{(N-j-1)!} - 9 \sum_{k=j}^{N-1} \frac{N^k}{(k-j)!} - \frac{(2\nu+3)^2 N^N}{(N-j)!} \right\}. \tag{C14}
\end{aligned}$$

For  $\ell = 2$ , (C12)–(C14) are verified to reduce to (C9). □

The calculation of  $g_{1+}$  may seem more difficult conceptually, involving analytic continuation in  $r$ . It actually is easier technically, since the exact form *does* follow from low-order asymptotics. The counterpart to (C6) reads

$$\frac{\gamma_5^2 g_1(r)}{2i\nu N^2} = \xi_5(r) \int^r dt \frac{t\xi_1(t)\xi_5(t)}{t-1} - \xi_1(r) \int_{-\infty}^r dt \frac{t\xi_5^2(t)}{t-1}, \tag{C15}$$

where the lower limit for the second term ensures  $g_1(r \rightarrow -\infty) \rightarrow 0$ . We select  $g_{1+}$  by continuing  $r$  from  $-\infty$  to the physical  $r > 1$  through the upper half plane. The remaining integration constant is made explicit as

$$\begin{aligned}
\frac{\gamma_5^2 g_1(r)}{2i\nu N^2} = & \xi_5(r) \left[ \int_{-\infty}^r \frac{dt}{t-1} \left( \xi_1(t)\xi_5(t) - \frac{\gamma_5}{N} \right) + \frac{\gamma_5 x}{N} + \alpha \right] \\
& - \xi_1(r) \int_{-\infty}^r dt \frac{t\xi_5^2(t)}{t-1}. \tag{C16}
\end{aligned}$$

Comparison to the differentiated asymptotics of  $g(\omega)$ ,

$$\frac{g_1(r)}{ie^{Nx/2}} = x - \frac{3x}{2\nu r} + \frac{3x}{Nr^2} + \frac{3}{\nu Nr} + O(r^{-2}), \tag{C17}$$

yields  $\alpha = \gamma_5/(4n^2 N^2)$  in  $O(r^0)$  of the last factor in

(C17); agreement of  $O(r^{-1})$  provides a check. □

### 3. Evaluation of the differentiated Wronskian

Substituting (C7) and (C17) into (C1), the prefactors of the  $t$ -integrals are all handled using (C5), yielding

$$\begin{aligned}
\frac{(2\nu+3)\gamma_5}{2i\nu N^2} J' = & \int_{-\infty}^r \frac{dt}{t-1} \left[ \frac{\gamma_5 - \gamma_3}{N} - \xi_3(t)\xi_5(t) \right] + \frac{\gamma_3 - \gamma_5}{4\nu^2 N^2} \\
& - \gamma_5 N^{-2} + \beta + C(r) + (\gamma_3 + \gamma_5)B(r) \\
& + \gamma_3 \gamma_5 D(r) + 2\gamma_3 N^{-1}x. \tag{C18}
\end{aligned}$$

Differentiating with respect to  $r$ , the  $r$ -independence of (C18) is readily verified. Indeed, the rhs is merely a regularized  $\int_1^{-\infty} dt \xi_3 \xi_5 t/(t-1)$ , which unfortunately diverges at both ends. Choosing  $r \rightarrow -\infty$ , the first term vanishes.

Inspecting (C8), it is gratifying that the individual exponential divergences (for  $r \rightarrow -\infty$ ) in  $B$ ,  $C$ , and  $D$  indeed cancel in (C18). Taking the  $t$ -contours in the upper half plane fixes the contributions of the singularities at  $t = 0, 1$ , yielding  $\text{Re } J'_+$  as in (3.13). In full, one has

$$\begin{aligned}
\lim_{r \rightarrow -\infty + i\eta} [C(r) + (\gamma_3 + \gamma_5)B(r) + \gamma_3 \gamma_5 D(r) + 2\gamma_3 N^{-1}x] = & \\
& \frac{2\gamma_3}{N} \left( \frac{\gamma_3}{\gamma_5} - 2 \right) (\gamma_E + \ln N) - 9 \text{Ei}(-N) + \frac{4\gamma_3^3}{9N^2 \gamma_5} \text{Ei}(N+i\eta) + 2\pi i \frac{\gamma_3}{N} \left( 1 - \frac{\gamma_3}{\gamma_5} \right) \\
& + \sum_{j=1}^{N-1} \frac{9}{j} \left[ \frac{\gamma_5}{2\nu^2 N} - e^{-N} \sum_{k=j}^{N-2} \frac{N^k}{k!} \right] + \frac{3\gamma_3(2^N - 1)}{(2\nu+3)N^2} + \frac{2(2\nu+3)(2\nu+5)(8\nu^2 + 8\nu - 3)\gamma_3}{9N^2(N-1)(N-2)} \\
& + \frac{2\gamma_3}{N^2} + \frac{(9-6\nu)\gamma_3}{2\nu^2} \frac{N-3}{N-2} - \frac{9\gamma_3 \gamma_5 e^N}{4\nu^4} \sum_{j=0}^{N-4} \frac{j!}{N^{j+3}} - \frac{(12\nu+9)\gamma_3 N^N e^{-N}}{\gamma_5} \sum_{j=1}^N \frac{1}{j j! (N-j)!} \\
& + \frac{3(2\nu+3)\gamma_5}{4\nu^2 N^2} + \frac{2\gamma_3}{N} \sum_{j=1}^{N-2} \frac{1}{j} - \frac{9\gamma_3 e^{-N}}{\gamma_5} \sum_{j=1}^{N-1} \sum_{k=1}^j \frac{N^j}{k k! (j-k)!} + \frac{9\gamma_3}{\nu^2} \sum_{j=3}^{N-2} \sum_{k=0}^{j-3} \frac{N^{j-k-2} k!}{j!} \\
& + \frac{4\nu \gamma_3 e^{-N}}{\gamma_5} \sum_{j=0}^{N-4} j! [(\nu+3)N^N \sigma_{j+3} - \nu N^{N-1} \sigma_{j+2}] - \frac{9\gamma_3 e^{-N}}{\gamma_5} \sum_{j=1}^{N-5} N^{N+j} \sigma_{j+3} \sum_{k=0}^{j-1} \frac{k!}{N^k}, \tag{C19}
\end{aligned}$$

with  $\sigma_j \equiv \sum_{k=j}^{N-2} [k!(N-2+j-k)!]^{-1}$ . The infinitesimal  $\eta > 0$  selects the upper branch of  $\text{Ei}(N+i\eta)$ .

Finally, Eqs. (3.11), (3.12), (C12)–(C14), and (C18)–(C19) combined yield a tedious, but explicit exact result for  $J'_+$ ; some cancellation occurs. For  $\ell = 2$ , one has

$$\begin{aligned} J'_+ = & \frac{i}{49 \cdot 2^{38}} \left[ -17122265640585(\gamma_E + \ln 8 - i\pi) \right. \\ & - 245810518235861775 \text{Ei}(8+i\eta) e^{-8} \\ & \left. + 36326230655979688 \right]. \end{aligned} \quad (\text{C20})$$

---

\* Corresponding author;  
electronic address: [alec@dwavesys.com](mailto:alec@dwavesys.com)

[1] A.A. Abramovici et al., *Science* **256**, 325 (1992).

[2] S. Chandrasekhar and S. Detweiler, *Proc. R. Soc. Lond. A* **344**, 441 (1975).

[3] V. Ferrari and B. Mashhoon, *Phys. Rev. D* **30**, 295 (1984).

[4] H.P. Nollert, *Phys. Rev. D* **47**, 5253 (1993).

[5] H. Liu, *Class. Quantum Grav.* **12**, 543 (1995).

[6] T. Regge and J.A. Wheeler, *Phys. Rev.* **108**, 1063 (1957).

[7] F.J. Zerilli, *Phys. Rev. D* **9**, 860 (1974).

[8] S. Chandrasekhar, *The Mathematical Theory of Black Holes* (Oxford University Press, 1983).

[9] P.T. Leung et al., *J. Math. Phys.* **42**, 4802 (2001).

[10] E.S.C. Ching et al., *Phys. Rev. Lett.* **74**, 2414 (1995); *Phys. Rev. D* **52**, 2118 (1995).

[11] A. Bachelot and A. Motet-Bachelot, *Ann. Inst. Henri Poincaré A* **59**, 3 (1993).

[12] E.W. Leaver, *Phys. Rev. D* **34**, 384 (1986).

[13] E.S.C. Ching et al., *Phys. Rev. Lett.* **74**, 4588 (1995); *Phys. Rev. D* **54**, 3778 (1996).

[14] Thus,  $\chi(x \rightarrow -\infty, \omega) \sim (\omega - \omega_n) e^{-i\omega x}$ , and one concludes that  $\chi(\omega_n)$  actually is the asymptotically *small* solution, i.e.,  $\chi(\omega_n) \propto f(-\omega_n)$  [15]. This equality “outgoing=incoming” may go against the intuition that these two kinds of waves should move in opposite directions. However, since the RWE is second-order in time, the waves  $\psi$  only “move” once, in the spirit of Hamiltonian mechanics, their momenta  $\hat{\psi}$  are specified [9]. One has  $\hat{\chi}(\omega_n) = -i\omega_n \chi(\omega_n)$  but  $\hat{f}(-\omega_n) = i\omega_n f(-\omega_n)$ , so even though  $\chi$  and  $f$  are proportional, the two-component *pairs* specifying a time evolution differ.

[15] A. Maassen van den Brink, *Phys. Rev. D* **62**, 064009 (2000).

[16] P.T. Leung, A. Maassen van den Brink, K.W. Mak, and K. Young, gr-qc/0301018, to appear in *Class. Quantum Grav.*

[17] P.T. Leung et al., *Phys. Lett. A* **247**, 253 (1998).

[18] The cut in Leaver’s series is studied at the end of Ref. [15], Section VI. However, besides the indicated factors, the normalization of  $g(x, \omega)$  is readily verified to branch at  $\omega = 0$  as well, so (6.7) in [15] does not immediately lead to a series for  $\Delta g$ . Thus, while computations *on* the NIA may be possible in future (cf. Section IV), the present indirect route is the state of the art.

[19] A. Maassen van den Brink, gr-qc/0303095.

[20] One has  $q'(\Gamma) = -8\pi\nu^2[2N(\gamma_3 - \gamma_5)/\gamma_5^2 + 4\gamma_3^2/9\gamma_5^2]$ , with  $\gamma_3, \gamma_5$  as in (3.11) and (3.12) respectively; see (8.2) in [15].

Since  $\gamma_5 \sim -\sqrt{3/2\pi}N^2$  while  $\gamma_3 = O(N)$  for  $\ell \rightarrow \infty$ , the latter can be neglected asymptotically, yielding the result at the end of Section II B.

[21] G.M. Murphy, *Ordinary Differential Equations and Their Solutions* (D. Van Nostrand, 1960).

[22] L.J. Slater, *Confluent Hypergeometric Functions* (Cambridge University Press, 1960).

[23] H. Onozawa, *Phys. Rev. D* **55**, 3593 (1997).

[24] Several additional complications arise. First, black holes also have total-transmission modes (TTMs), defined by  $\psi \propto e^{+i\omega x}$  for  $|x| \rightarrow \infty$  (i.e., *in* from the left and *out* to the right), whereas QNMs satisfy OWCs. TTMs and QNMs, defined by zeros of different Wronskians [9], are in general unrelated. Second, however, at the anomalous points the two conditions agree [15] (see also Appendix B). Then TTMs can coincide with QNMs, refuting that they “will never coalesce in general” ([23], end of Section III). Third, the transformations between the ZE (polar) and RWE (axial sector), or between the spin  $s = \pm 2$  sectors of the Teukolsky equations also valid for  $a \neq 0$ , are degenerate at the algebraically special frequency  $\Omega(a)$ , with  $\Omega(0) = -i\Gamma$ . Thus, the two spectra may differ at  $\Omega(a)$ , but often the exception is not emphasized and the QNM spectrum stated without specifying the sector. In fact,  $\Omega(a)$  corresponds to a family of TTMs, and, even more subtle, *does* collide with a family of QNMs precisely for  $a \rightarrow 0$  [i.e., at the anomalous (miraculous) point of the ZE (RWE)]. All these call for a separate careful study of the rotating case.

[25] By (4.6) in Ref. [9], for a Witten index  $\chi = 0$ .

[26] I.M. Gelfand and B.M. Levitan, *Am. Math. Soc. Transl.* **1**, 253 (1951). For other references and numerics see, e.g., W. Rundell and P.E. Sacks, *Math. Comput.* **58**, 161 (1992); C.-P. Sun, K. Young, and J. Zou, *J. Phys. A: Math. Gen.* **32**, 3833 (1999).

[27] G. Pöschl and E. Teller, *Z. Phys.* **83**, 143 (1933); V. Cardoso and J.P.S. Lemos, *Phys. Rev. D* **67**, 084020 (2003); A. Maassen van den Brink, gr-qc/0304092, to appear in *Phys. Rev. D*.

[28] E. Berti, V. Cardoso, K.D. Kokkotas, and H. Onozawa, gr-qc/0307013.

[29] E.W. Leaver, *J. Math. Phys.* **27**, 1238 (1986).

[30] F.W.J. Olver, *Math. Comput.* **18**, 65 (1964); Y.T. Liu, Thesis (The Chinese University of Hong Kong, 1997).

[31] G. Jaffé, *Z. Phys.* **87**, 535 (1934).

[32] N.B.: Maple V mishandles exponential integrals, especially their series expansions.